Mathematics

https://www.aimspress.com/journal/Math

AIMS Mathematics, 11(7): 22205–22232.
DOI: 10.3934/math.2026899
Received: 19 May 2026
Revised: 06 July 2026
Accepted: 14 July 2026
Published: 24 July 2026

Research article

Dynamical behaviors of the (3+1)-dimensional nonlinear wave equation in gas-bubble-containing liquid

Miaomiao Li and Zenggui Wang*

School of Mathematical and Systems Sciences, Liaocheng University, Liaocheng 252059, China

* **Correspondence:** Email: wangzenggui@lcu.edu.cn.

Abstract: In this paper, we investigated the (3+1)-dimensional nonlinear wave equation in gas-bubble-containing liquid, which can delineate the dynamic behaviors of waves in the mechanics of fluids. It plays a crucial role in explaining the propagation of weakly nonlinear waves, which are commonly encountered in natural sciences, medicine, fluid mechanics, and engineering. Based on the bifurcation method, the dynamical behavior of the reduced system was performed through the phase portrait. By using different parametric conditions, new soliton wave solutions were derived, including periodic wave-type, periodic breaking wave-type, solitary wave-type, and unbounded wave-type solutions. Additionally, the visualizations of the obtained exact solutions were employed to present the wave behavior of the equation. It is of great importance for understanding the inherent evolution laws of nonlinear waves in bubbly media within fluid dynamics. To ensure stability for the solutions, a sensitivity analysis was performed within a framework for a dynamical system, as well as sensitivities for parameters to the points of equilibrium. The orbital structures are discussed. Furthermore, the chaotic behavior of the equation under external periodic forcing was also investigated, and the existence of periodic motions was verified via Lyapunov exponents. Compared with the literature, for the first time, we adopt the bifurcation method of dynamical systems to solve the equation and obtained novel exact solutions.

Keywords: (3+1) D-nonlinear wave equation; bifurcation analysis; soliton solutions; sensitivity analysis; quasi periodic
Mathematics Subject Classification: 34D08, 35Q53, 35C08, 37G10

1. Introduction

Nonlinear partial differential equations can delineate abundant propagation characteristics and the nonlinear phenomena of waves, serving mathematical models' role for nonlinear behaviors of science and for engineering such as physics [1], ocean dynamics [2], fluid mechanics, quantum mechanics, biological [3], nonlinear optics [4], nanofluids, geometry [5], and economics. Liquids with entrained gas bubbles [6, 7] are common in many fields of study, including medicine and engineering, and are nonlinear phenomena in nature. Research on bubble-containing liquids have always been a research hotspot of nonlinear wave studies. Bubbly liquids are widely applied in science, chemistry, physics, the field of nature, and diurnal life, attracting extensive attention. Having an in-depth comprehension of the nonlinear and dynamics behavior of shock waves during the formation process is crucial for enhancing these industrial uses, enabling an in-depth investigation of bubble generation and interactions under various conditions, thereby helping to design more effective strategies for industrial process optimization.

To derive various forms of exact solutions, researchers have attempted to seek solutions to PDEs by means of various approaches. For instance, Wang et al. [8] first used the bilinear method to construct a lump-stripe composite soliton and hybrid rogue wave solutions of the (3+1)-dim nonlinear wave equation in bubbly liquids. Liu and Zhang [9] used the principle of linear combination and the method of generalized homoclinic orbit to analyze the generalized composite solutions and rogue wave solutions of the nonlinear wave equation. In [10], Mohamed used a symbolic computation approach to analyze the equation of the (3+1)-dim nonlinear gas bubbles model. In [11], Abeer used the extended F-expansion method to analyze the general-form nonlinear (3+1)-dim wave equation of bubble-containing liquids. In [12], Min explored a generalized (3+1)-dim DS equation governed by nonlinearity of parabolic type thorough dynamical systems analysis and Lie group theory. In [13], Xin explored the (2+1)-dim Sakovich equation with variable coefficients and adopted Lie symmetry analysis to obtain the periodic wave form and collision profile of two solitons. In [14], Ehab used a canonical set of Lie symmetry analysis to obtain exact solutions of the soliton form to the equation of (3+1)-dim generalized nonlinear wave. There are also other approaches, including the homogeneous balance approach in [15, 16], the Darboux transformation method in [17, 18], the exp-function method in [19], the special solution substitution method of the Riccati equation in [20], the method of elliptic function [21, 22], the elliptic function of Jacobi type approach discussed in [23], the hyperbolic cosine method in [24, 25], and the Hirota bilinear method in [26–28]. Some new invariant solutions were found using classical and non-classical Lie group analyses in [29, 30], and so on.

A generalized three spatial and one temporal dimension nonlinear wave equation in gas-bubble liquid was considered by Kudryashov [31],

$$\left(u_t + uu_x + \frac{1}{4}u_{xxx} - u_x\right)_x + \frac{3}{4}\left(u_{yy} + u_{zz}\right) = 0. \tag{1.1}$$

In [32], Shalini used Lie symmetry to construct group-invariant solutions of (1.1). Based on the similarity reduction method, more than 30 types of novel exact solutions are deduced. In [33], by using the Hirota bilinear method, Liu obtained the lump solution representations and the interaction solutions between lumps and solitons of a generalized (3+1)-dimensional variable-coefficient nonlinear-wave equation in liquid with gas bubbles:

$$\alpha(t)u_x^2 + \alpha(t)uu_{xx} + \beta(t)u_{xxxx} + \gamma(t)u_{xx} + \delta(t)u_{yy} + \varrho(t)u_{zz} + u_{xt} = 0. \tag{1.2}$$

In [34], Shen adopted the Hirota bilinear method and the bilinear Bäcklund transformation and symbolic calculation techniques to consider

$$(u_t + h_1uu_x + h_2u_{xxx} + h_3u_x)_x + h_4u_{yy} + h_5u_{zz} = 0. \tag{1.3}$$

The traveling wave solutions and hybrid solutions, together with the center-controllable rogue wave solutions of high order of the first, second, and third order, are obtained. In [35], Wang used the Hirota bilinear method to consider

$$(u_t + h_1 u u_x + h_2 u_{xxxx} + h_3 u_x)_x + h_4 u_{yy} + h_5 u_{zz} = 0. \tag{1.4}$$

The primary lump, solutions of secondary lump, and two kinds of solutions of mixed interaction between lumps and single solitons are obtained. In [36], Ehab employed the Lie symmetries method for

$$(u_t + a_2 u_{xxx} + a_1 u u_x + a_3 u_x)_x + a_4 u_{yy} + a_5 u_{zz} = 0, \tag{1.5}$$

and obtained novel exact solutions, including soliton-type solutions, periodic solutions, logarithmic solutions, exponential solutions, polynomial solutions, and group-invariant solutions containing arbitrary functions. In [37], Adeyemo and Khalique also used the Lie symmetry method to construct soliton solutions of the equation

$$(u_t + b_1 u_x + b_2 u u_x + b_3 u_{xxxx})_x + b_4 u_{yy} + b_5 u_{zz} = 0. \tag{1.6}$$

In [38], Kumar employed the approach of generalized exponential rational functions to obtain finite-form soliton solutions, including various wave profiles such as dark solitons, multi-wave structured solitons, kink solitons, bright solitons, combined singular solitons, and singular solitons. In [39], Alizadeh used the classical and non-classical Lie symmetries and the bifurcation method to obtain a triangular function type, periodic wave, hyperbolic functional, rational-function, kink wave, and solitary solutions. In [40], Wazwaz et al. used Painlevé Integrability analysis to construct the solitary waves of (1.6).

The bifurcation method [41, 42] is an efficient method to investigate the solutions for nonlinear PDEs, such as the nonlinear Schrödinger equation and other non-linear wave equations [43, 44]. Compared with other methods, the bifurcation method has a distinct advantage: intuitive visualization. We can determine the types of orbits and their corresponding exact solutions according to the morphological features of orbits in phase portraits. Different parameters correspond to distinct orbits, and the associated exact solutions will change as the parameters vary. To our knowledge, the bifurcation behavior of (1.1) has yet to be investigated. Accordingly, we use the bifurcation approach to construct the exact traveling wave solutions of (1.1).

We structure this paper as follows: In Section 2, the method of bifurcation for dynamical systems is adopted to derive a corresponding planar system of (1.1), and the phase plane analysis about the system are plotted. Section 3 exhibits exact traveling wave solutions under three cases, as well as 3D visual graphs, 2D density graphs, and time slice graphs associated with certain exact solutions. In Section 4, we provide interpretations for the obtained exact solutions. In Section 5, by adjusting the parameters, the influences on the equilibrium points and orbital patterns are analyzed, and we conduct the analysis of sensitivity of the equation. In Section 6, we first analyze the periodic and quasi-periodic behaviors of the equation, and then investigate the chaotic dynamics of the system via Lyapunov characteristic exponents. Finally, a conclusion of this paper is given in Section 7.

2. Phase portraits and bifurcation analysis

Assume (1.1) has a traveling wave solution,

$$u(\xi) = u(kx + ly + mz - ct), \quad \xi = kx + ly + mz - ct, \tag{2.1}$$

in which k, l, m, c are traveling wave parameters, and c represents the wave velocity. Substituting (2.1) into (1.1) yields

$$\frac{1}{4}k^4 u'''' + k^2(u')^2 + k^2 uu'' + \left(-ck - k^2 + \frac{3}{4}l^2 + \frac{3}{4}m^2\right)u'' = 0. \tag{2.2}$$

Performing integration of (2.2), we get

$$\frac{1}{4}k^4 u''' + k^2 uu' + \left(-ck - k^2 + \frac{3}{4}l^2 + \frac{3}{4}m^2\right)u' = c_0, \tag{2.3}$$

where c_0 is a constant and let $c_0 = 0$. Then, performing integration of (2.3), we get

$$\frac{1}{4}k^4 u'' + \frac{1}{2}k^2 u^2 + \left(-ck - k^2 + \frac{3}{4}l^2 + \frac{3}{4}m^2\right)u = c_1, \tag{2.4}$$

in which c_1 is a constant.

Assume $A = -2k^{-2}$, $B = 4k^{-4}\left(-ck - k^2 + \frac{3}{4}l^2 + \frac{3}{4}m^2\right)$, and $C = 4c_1 k^{-4}$, and let $\frac{du}{d\xi} = y$, then (2.4) reduces to the following dynamical systems

$$\begin{cases} \dfrac{du}{d\xi} = y, \\ \dfrac{dy}{d\xi} = Au^2 - Bu + C. \end{cases} \tag{2.5}$$

The constant C in system (2.5) is an integration constant obtained after performing the traveling wave transformation and two successive integrations on the original equation. At this stage, no specific boundary conditions are imposed, and c_0, c_1, and C are all arbitrary constants. However, when solving for exact solutions, we take the far-field condition at infinity as the boundary condition to fix the value of C for plotting bifurcation phase portraits.

In addition, C is not a Hamiltonian conserved quantity, yet it serves as an external parameter governing bifurcation structures. Different values of C alter the overall structure of phase orbits and the distribution of equilibrium points. The types of traveling waves supported by this physical model can be determined from distinct bifurcation phase portraits. When $C = 0$, no fluid displacement occurs, corresponding to the baseline background state as illustrated in Figure 1(d). When $C \neq 0$, this leads to fluid displacement, as shown in Figure 1(a)–(g). Therefore, C characterizes the displacement magnitude of the background state.

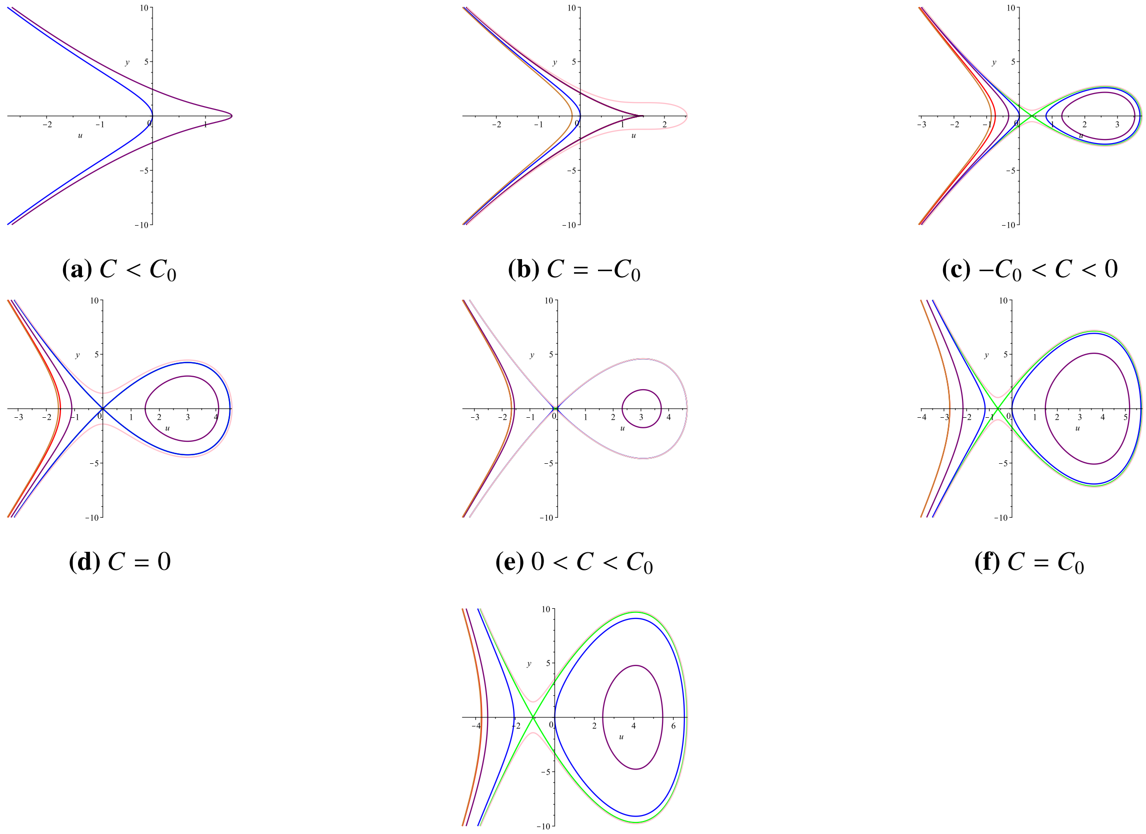

(a) $C < C_0$ **(b)** $C = -C_0$ **(c)** $-C_0 < C < 0$ **(d)** $C = 0$ **(e)** $0 < C < C_0$ **(f)** $C = C_0$ **(g)** $C > C_0$

Figure 1. Phase diagrams of (2.5) for $k = 1$, $l = 1$, $m = 1$, $c = 2$: (a) $C = -5$; (b) $C = -4.5$; (c) $C = -2$; (d) $C = 0$; (e) $C = 0.5$; (f) $C = 4.5$; and (g) $C = 9$.

Compute the first integral of system (2.5),

$$H(u, y) = \frac{1}{2}y^2 - \frac{1}{3}Au^3 + \frac{1}{2}Bu^2 - Cu = h, \tag{2.6}$$

in which h is a Hamilton constant.

In [45], the Hamiltonian $H(x, y)$ can be interpreted as the total energy of the system, which equals the sum of kinetic energy and potential energy. All orbits obey the Hamiltonian conservation law, and Hamiltonian H remains constant along every solution trajectory. Consequently, the equilibrium points of such systems can be only saddles or centers, and H is a first integral of the system.

To investigate the stability of the Hamiltonian system proposed in this paper, we construct the bifurcation phase portraits of system (2.5) based on the relationship between the parameter C and the critical value C_0. Furthermore, the bifurcation phase portraits derived from the Hamiltonian system not only enable us to intuitively identify the types of orbits and exact solutions, but also enable us to derive the orbital equations and corresponding exact analytical solutions.

Next, we analyze the dynamical system (2.5) about the phase portrait bifurcation. Define

$$f(u) = Au^2 - Bu + C, \tag{2.7}$$

and

$$f_0(u) = Au^2 - Bu. \tag{2.8}$$

It is clear that function (2.8) has two zeros,

$$u_0^* = 0,\ u_1^* = \frac{B}{A}, \tag{2.9}$$

and has an extreme point given by

$$u^* = \frac{B}{2A}. \tag{2.10}$$

This gives rise to the extreme value C_0 of the function $f_0(u)$,

$$C_0 = |f_0(u^*)| = \left|-\frac{B^2}{4A}\right|. \tag{2.11}$$

Let

$$F_0 = |f_0(u^*)| = C - \frac{B^2}{4A}. \tag{2.12}$$

It is clear that F_0 is the extreme value of (2.7). The phase portrait of system (2.5) with varying parameters through qualitative analysis [46, 47] is illustrated in Figure 1.

Figure 1(a) shows sharp corners. A bifurcation diagram featuring sharp corners is also presented in [48]. Both cases involve contour lines or streamlines with discontinuous first derivatives at a single point, lacking smooth circular arc transitions and forming abruptly bent sharp corners. They both correspond to critical bifurcation states where singular points coincide, and the topological trajectories on either side of the sharp corners are distinct.

Furthermore, despite the presence of sharp corners in both cases, obvious discrepancies can be identified. In [48], the researchers conducted a detailed investigation of the flow beneath solitary waves propagating on an exponentially decaying sheared current. The structural evolution is governed by the magnitude of the underlying current parameter a. As parameter a is varied, the two saddle points collide on the bottom boundary and merge into a single saddle point. This is followed by a collision between a saddle point and a center point, which generates a streamline with a sharp crest. This phenomenon occurs at the critical value of the control parameter, featuring two real stationary points and representing physical streamlines of actual water waves. In contrast, we study the (3+1)-dimensional nonlinear wave equation for liquids containing gas bubbles. The bifurcation diagram herein is derived from a Hamiltonian system and determined by the values of system parameters A–C. Moreover, the singular points obtained are a pair of complex conjugate singularities without physical fluid-dynamic interpretations.

Assume that $(u_i, 0)$ is an equilibrium point of the (2.5). Then, the eigenvalues of the system (2.5) at this point are given by

$$\lambda_i = \pm\sqrt{f'(u_i)}. \tag{2.13}$$

From the theory of qualitative analysis for differential equations [46], we have:

(1) If $f'(u_i) = 0$, $(u_i, 0)$ is a degenerate saddle.

(2) If $f'(u_i) > 0$, $(u_i, 0)$ is a saddle point.

(3) If $f'(u_i) < 0$, $(u_i, 0)$ is a center.

Homoclinic orbits correspond to solutions of the solitary wave, heteroclinic orbits are linked to solutions of the kink wave or anti-kink wave, periodic orbits correspond to solutions of the periodic wave, and bounded orbits correspond to solutions of the breaking wave.

When $C < 0$ for the dynamical system in this paper, equilibrium points exist if and only if $\Delta \geq 0$. There are two equilibrium points $E_1 = \frac{B+\sqrt{B^2-4AC}}{2A}$ and $E_2 = \frac{B-\sqrt{B^2-4AC}}{2A}$:

(1) If $\Delta > 0$, E_1 is a saddle point, E_2 is a center.

(2) If $\Delta = 0$, E_1 is a degenerate saddle as well as E_2 is a saddle point.

When $C = -C_0 = -\left|\frac{B^2}{4A}\right| \neq 0$:

(1) If $A > 0, B > 0$, $E_3 = (\frac{B}{2A} + \frac{B}{\sqrt{2}A}, 0)$ is a saddle point, $E_4 = (\frac{B}{2A} - \frac{B}{\sqrt{2}A}, 0)$ is a center.

(2) If $A > 0, B < 0$, $E_5 = (-\frac{B}{2A} - \frac{B}{\sqrt{2}A}, 0)$ and $E_6 = (-\frac{B}{2A} + \frac{B}{\sqrt{2}A}, 0)$ are saddle points.

(3) If $A \neq 0, B = 0$, $E_7 = E_8 = (0, 0)$ are degenerate saddle.

(4) If $A < 0, B > 0$, $E_9 = (-\frac{B}{2A} + \frac{B}{\sqrt{2}A}, 0)$ and $E_{10} = (-\frac{B}{2A} - \frac{B}{\sqrt{2}A}, 0)$ are centers.

(5) If $A < 0, B < 0$, $E_{11} = (\frac{B}{2A} - \frac{B}{\sqrt{2}A}, 0)$ is a saddle point, $E_{12} = (\frac{B}{2A} + \frac{B}{\sqrt{2}A}, 0)$ is a center.

When $-C_0 < C < 0$, equilibrium points exist if and only if $\Delta \geq 0$, there exist two equilibrium points $E_{13} = \frac{B+\sqrt{B^2-4AC}}{2A}$ and $E_{14} = \frac{B-\sqrt{B^2-4AC}}{2A}$:

(1) If $\Delta > 0$, E_{13} is a saddle point, E_{14} is a center.

(2) If $\Delta = 0$, two equilibrium points are degenerate saddle points.

When $C = 0$ for the dynamical system in this paper, there exist two points that are in equilibrium $E_0^* = (u_0^*, 0) = (0, 0)$ and $E_1^* = (u_1^*, 0) = \left(\frac{B}{A}, 0\right)$:

(1) If $A \neq 0, B > 0$, E_0^* is a center and E_1^* is a saddle point.

(2) If $A \neq 0, B < 0$, E_0^* is a saddle point and E_1^* is a center.

(3) If $A \neq 0, B = 0$, two equilibrium points are degenerate saddle points.

When $0 < C < C_0$, equilibrium points exist if and only if $\Delta \geq 0$, there are two equilibrium points $E_{15} = \frac{B+\sqrt{B^2-4AC}}{2A}$ and $E_{16} = \frac{B-\sqrt{B^2-4AC}}{2A}$:

(1) If $\Delta > 0$, E_{15} is a saddle point as well as the E_{16} is a center.

(2) If $\Delta = 0$, both are degenerate saddle points.

When $C = C_0 = \left|\frac{B^2}{4A}\right| \neq 0$:

(1) If $A > 0, B > 0$, $E_{17} = E_{18} = (\frac{B}{2A}, 0)$ are degenerate saddle points.

(2) If $A > 0, B < 0$, $E_{19} = E_{20} = (-\frac{B}{2A}, 0)$ are degenerate saddle points.

(3) If $A \neq 0, B = 0$, $E_{21} = E_{22} = (0, 0)$ are degenerate saddle points.

(4) If $A < 0, B > 0$, $E_{23} = (-\frac{B}{2A} + \frac{B}{\sqrt{2}A}, 0)$ and $E_{24} = (-\frac{B}{2A} - \frac{B}{\sqrt{2}A}, 0)$ are centers.

(5) If $A < 0, B < 0$, $E_{25} = (\frac{B}{2A} - \frac{B}{\sqrt{2}A}, 0)$ is a saddle point, $E_{26} = (\frac{B}{2A} + \frac{B}{\sqrt{2}A}, 0)$ is a center.

When $C > C_0$, equilibrium points exist if and only if $\Delta \geq 0$. $E_{27} = \frac{B+\sqrt{B^2-4AC}}{2A}$ and $E_{28} = \frac{B-\sqrt{B^2-4AC}}{2A}$ are equilibrium points:

(1) If $\Delta > 0$, E_{27} is a saddle point and E_{28} is a center.

(2) If $\Delta = 0$, two equilibrium points are degenerate saddle points.

3. Exact traveling wave solution

Based on (2.5) and (2.6), we obtain

$$y^2 = \frac{2}{3}Au^3 - Bu^2 + 2Cu + 2h, \tag{3.1}$$

$$\frac{du}{\sqrt{\psi(u)}} = d\xi, \tag{3.2}$$

in which

$$\psi(u) = \frac{2}{3}Au^3 - Bu^2 + 2Cu + 2h. \tag{3.3}$$

The exact traveling wave solutions with the parameter values $A < 0, B < 0$, and $C = 0$ in Figure 1(d) are considered.

(1) When $h = h_1 = 0$, we obtain a pair of homoclinic orbits with symmetry Γ_1' and Γ_1'' above the a point that functions as a saddle $(0, 0)$ as well as one special orbit Γ_1^* ,

$$\Gamma_1',\ \Gamma_1'',\ \Gamma_1^*:\ y = \pm\sqrt{\frac{2}{3}Au^2(u_1 - u)}, \tag{3.4}$$

in which $u_1 = \frac{B}{A}$. Substituting (3.4) into (3.2) and integrating along the orbits Γ_1' , Γ_1'' , and Γ_1^* , respectively, yields

$$\pm\int_u^0 \frac{1}{\sqrt{\frac{2}{3}As^2(u_1 - s)}}\,ds = \xi, \quad u < 0 < u_1, \tag{3.5}$$

$$\pm\int_0^{u_1} \frac{1}{\sqrt{\frac{2}{3}As^2(u_1 - s)}}\,ds = \xi, \quad 0 < u < u_1. \tag{3.6}$$

We obtain the solitary wave solution

$$u_{1,2\pm} = -\frac{1}{2}B\left(\operatorname{sech}^2\left(\frac{1}{2}\sqrt{-\frac{1}{6}AB}\,\xi\right)\right), \tag{3.7}$$

and an unbounded wave solution

$$u_{3\pm} = -\frac{1}{2}B\left(1 - \coth^2\left(\frac{1}{2}\sqrt{-\frac{1}{6}AB}\,\xi\right)\right). \tag{3.8}$$

(2) When $h = h_2 = -9$, there is the special orbit Γ_2 crossing the points $(u_1^*, 0)$,

$$\Gamma_2:\ y = \pm\sqrt{\frac{2}{3}A(u - u_1^*)(u - d_1)^2}, \quad u < u_1^*, \tag{3.9}$$

where d_1 and d_2 are complex number. We substitute (3.9) into (3.2) and integrate along the orbit Γ_2 , which yields

$$\pm\int_u^{u_1^*} \frac{ds}{\sqrt{\frac{2}{3}A(s - u_1^*)s^2}} = \xi. \tag{3.10}$$

The solutions of the periodic breaking wave of (1.1) is given by

$$u_{4\pm} = -\frac{3\sqrt{\Delta}}{2A}\left[1 - \csc^2\left(\frac{1}{2}\Delta^{\frac{1}{4}}\xi\right)\right] + \frac{B + \sqrt{\Delta}}{2A}, \tag{3.11}$$

in which $\Delta = B^2 - 4AC$.

(3) When $h = 0$, the orbital color in this case is blue, the same as that in (1).

(4) When $h = -4.5$, we obtain the closed orbit Γ_3 crossing the points $(u_2, 0)$ and $(u_3, 0)$, and special orbit Γ_3^* proceeds through the point $(u_4, 0)$,

$$\Gamma_3: \ y = \pm\sqrt{(u-u_2)(u-u_3)(u_4-u)}, \quad u_4 < u_3 < u < u_2, \tag{3.12}$$

$$\Gamma_3^*: \ y = \pm\sqrt{(u_2-u)(u_3-u)(u_4-u)}, \quad u < u_4 < u_3 < u_2. \tag{3.13}$$

Substituting (3.12) and (3.13) into (3.2) and integrating along the orbits Γ_3 and Γ_3^*, respectively, yield

$$\pm\int_{u_3}^{u_2} \frac{ds}{\sqrt{\frac{2A}{3}(s-u_2)(s-u_3)(u_4-s)}} = \xi, \tag{3.14}$$

$$\pm\int_{u}^{u_4} \frac{ds}{\sqrt{\frac{2A}{3}(u_2-s)(u_3-s)(u_4-s)}} = \xi. \tag{3.15}$$

Then we get the solutions of periodic wave

$$u_{5\pm} = u_2 + (u_3 - u_2)\,\mathrm{sn}^2\left(\sqrt{\frac{|A|(u_2-u_4)}{6}}\xi, \ \sqrt{\frac{u_3-u_2}{u_4-u_2}}\right), \tag{3.16}$$

and a periodic breaking wave solution

$$u_{6\pm} = u_2 + \frac{u_3 - u_2}{\mathrm{sn}^2\left(\sqrt{\frac{|A|(u_2-u_4)}{6}}\xi, \ \sqrt{\frac{u_3-u_2}{u_4-u_2}}\right)}. \tag{3.17}$$

(5) When $h = -10$, we obtain that there is the special orbit Γ_4 crossing the point $(u_5, 0)$,

$$\Gamma_4: \ y = \pm\sqrt{\frac{2}{3}A(u-u_5)(u-d_2)^2}, \quad u < u_5. \tag{3.18}$$

Substituting(3.18) into (3.2) and integrating along the orbit Γ_4 yields

$$\pm\int_{u}^{u_5} \frac{ds}{\sqrt{\frac{2}{3}A(s-u_5)(s-d_2)^2}} = \xi. \tag{3.19}$$

Then we get the periodic breaking wave solution

$$u_{7\pm} = -\frac{3\sqrt{\Delta}}{2A}\left[1 - \csc^2\left(\frac{1}{2}\Delta^{\frac{1}{4}}\xi\right)\right] + \frac{B + \sqrt{\Delta}}{2A}. \tag{3.20}$$

Next, we investigate the exact solutions under the case where $A < 0$, $B < 0$, and $0 < C < C_0$ in Figure 1(e).

(1) When $h = h_1$, we obtain homoclinic orbits that are symmetric, Γ_6^+ and Γ_6^-, and the orbits with uniqueness Γ_6^* pass through the points $(u_6, 0)$ and $(u_7, 0)$,

$$\Gamma_6^+, \ \Gamma_6^-: \ y = \pm\sqrt{\frac{2}{3}A\,(u-u_6)^2\,(u_7-u)}, \quad u_6 < u < u_7, \tag{3.21}$$

$$\Gamma_6^*:\ y=\pm\sqrt{\frac{2}{3}A\,(u_6-u)^2\,(u_7-u)},\quad u<u_6<u_7. \tag{3.22}$$

Taking (3.21) and (3.22) into (3.2) and integrating along the orbits Γ_6^+, Γ_6^-, and Γ_6^*, respectively, yield

$$\pm\sqrt{\frac{3}{2|A|}}\int_{u_6}^{u_7}\frac{ds}{\sqrt{(s-u_6)^2(u_7-s)}}=\xi, \tag{3.23}$$

$$\pm\sqrt{\frac{3}{2|A|}}\int_{u}^{u_6}\frac{ds}{\sqrt{(u_6-s)^2(u_7-s)}}=\xi. \tag{3.24}$$

Then we derive the solitary solution wave

$$u_{8,9\pm}=\frac{1}{6}B\left(1-3\tanh^2\left(\frac{1}{2}\sqrt{\frac{1}{6}AB}\,\xi\right)\right), \tag{3.25}$$

and the unbounded wave solution

$$u_{10\pm}=\frac{1}{6}B\left(1-3\coth^2\left(\frac{1}{2}\sqrt{\frac{1}{6}AB}\,\xi\right)\right). \tag{3.26}$$

(2) When $h=h_2$, we know the special orbit Γ_7 crosses the point $(u_8,0)$,

$$\Gamma_7:\ y=\pm\sqrt{\frac{2}{3}A(u-d_3)^2(u_8-u)},\quad u<u_8. \tag{3.27}$$

Substituting (3.27) into (3.2) and integrating along orbit Γ_7 yields,

$$\pm\sqrt{\frac{3}{2|A|}}\int_{u}^{u_8}\frac{ds}{\sqrt{(s-d_3)^2(u_8-s)}}=\xi. \tag{3.28}$$

Then we derive the periodic breaking wave solution

$$u_{11\pm}=-\frac{3\sqrt{\Delta}}{2A}\left[1-\csc^2\left(\frac{1}{2}\Delta^{\frac{1}{4}}\xi\right)\right]+\frac{B+\sqrt{\Delta}}{2A}. \tag{3.29}$$

(3) When $h=0$, we have the closed orbit Γ_8 and special orbit Γ_8^* passing through the points $(u_9,0)$ and $(u_{10},0)$,

$$\Gamma_8:\ y=\pm\sqrt{\frac{2}{3}Au(u-u_9)(u_{10}-u)},\quad u_9<0<u<u_{10}, \tag{3.30}$$

$$\Gamma_8^*:\ y=\pm\sqrt{\frac{2}{3}Au(u_9-u)(u_{10}-u)},\quad u<u_9<0<u_{10}. \tag{3.31}$$

Taking (3.30) and (3.31) into (3.2) and integrating along orbits Γ_8 and Γ_8^*, respectively, yield

$$\pm\int_{0}^{u_{10}}\frac{ds}{\sqrt{\frac{2}{3}As(s-u_9)(u_{10}-s)}}=\xi, \tag{3.32}$$

$$\pm\int_{u}^{u_9}\frac{ds}{\sqrt{\frac{2}{3}As(u_9-s)(u_{10}-s)}}=\xi. \tag{3.33}$$

We derive the periodic breaking wave solution

$$u_{12\pm}=u_{10}+(-u_{10})\,\mathrm{sn}^2\left(\sqrt{\frac{|A|(u_{10}-u_9)}{6}}\xi,\ \sqrt{\frac{-u_{10}}{u_9-u_{10}}}\right), \tag{3.34}$$

and the unbounded wave solution

$$u_{13\pm}=u_{10}+\frac{-u_{10}}{\mathrm{sn}^2\left(\sqrt{\frac{|A|(u_{10}-u_9)}{6}}\xi,\ \sqrt{\frac{-u_{10}}{u_9-u_{10}}}\right)}. \tag{3.35}$$

(4) When $h=-9$, there is the closed orbit Γ_9 crossing the points $(u_{13},0)$ and $(u_{12},0)$ and special orbit Γ_9^* crossing the point $(u_{11},0)$,

$$\Gamma_9:\ y=\pm\sqrt{\frac{2}{3}A(u-u_{11})(u-u_{12})(u_{13}-u)},\quad u_{11}<u_{12}<u<u_{13}, \tag{3.36}$$

$$\Gamma_9^*:\ y=\pm\sqrt{\frac{2}{3}A(u_{11}-u)(u_{12}-u)(u_{13}-u)},\quad u<u_{11}<u_{12}<u_{13}. \tag{3.37}$$

We insert (3.36) and (3.37) into (3.2) and integrate orbits Γ_9 and Γ_9^*, respectively, yielding

$$\pm\sqrt{\frac{3}{2|A|}}\int_{u_{12}}^{u_{13}}\frac{ds}{\sqrt{(s-u_{11})(s-u_{12})(u_{13}-s)}}=\xi, \tag{3.38}$$

$$\pm\sqrt{\frac{3}{2|A|}}\int_{u}^{u_{11}}\frac{ds}{\sqrt{(u_{11}-s)(u_{12}-s)(u_{13}-s)}}=\xi. \tag{3.39}$$

We get the periodic wave solution

$$u_{14\pm}=u_{13}+(u_{12}-u_{13})\,\mathrm{sn}^2\left(\sqrt{\frac{|A|(u_{13}-u_{11})}{6}}\xi,\ \sqrt{\frac{u_{12}-u_{13}}{u_{11}-u_{13}}}\right), \tag{3.40}$$

and periodic breaking wave solution

$$u_{15\pm}=u_{13}+\frac{u_{12}-u_{13}}{\mathrm{sn}^2\left(\sqrt{\frac{|A|(u_{13}-u_{11})}{6}}\xi,\ \sqrt{\frac{u_{12}-u_{13}}{u_{11}-u_{13}}}\right)}. \tag{3.41}$$

(5) When $h=h_2-0.01$, we have the special orbit Γ_{11} crossing the points $(u_{14},0)$, $(u_{15},0)$, and $(u_{16},0)$,

$$\Gamma_{11}:\ y=\pm\sqrt{\frac{2A}{3}(u_{14}-u)(u-u_{15})(u-u_{16})},\quad u<u_{14}. \tag{3.42}$$

Substituting (3.42) into (3.2) and integrating along the orbit Γ_{11} yield

$$\pm\sqrt{\frac{3}{2|A|}}\int_{u}^{u_{14}}\frac{ds}{\sqrt{(u_{14}-s)(s-u_{15})(s-u_{16})}}=\xi. \tag{3.43}$$

We derive the periodic breaking wave solution

$$u_{16\pm} = -\frac{3\sqrt{\Delta}}{2A}\left[1-\csc^2\left(\frac{1}{2}\Delta^{\frac{1}{4}}\xi\right)\right]+\frac{B+\sqrt{\Delta}}{2A}. \tag{3.44}$$

Furthermore, we take into account $A < 0$, $B < 0$, and $C = C_0 = \left|\frac{B^2}{4A}\right|$ shown in Figure 1(f).

(1) When $h = h_1$, two homoclinic orbits are symmetric, Γ^+_{12} and Γ^-_{12} and the distinctive orbit Γ^*_{12} crosses the points $(u_{17}, 0)$ and $(u_{18}, 0)$,

$$\Gamma^+_{12},\ \Gamma^-_{12}:\ y = \pm\sqrt{(u-u_{17})^2(u_{18}-u)}, \quad u_{17} < u < u_{18}, \tag{3.45}$$

$$\Gamma^*_{12}:\ y = \pm\sqrt{(u_{17}-u)^2(u_{18}-u)}, \quad u < u_{17} < u_{18}. \tag{3.46}$$

Taking (3.45) and (3.46) into (3.2) and integrating along the orbits Γ^+_{12}, Γ^-_{12} and Γ^*_{12}, respectively, yield

$$\pm\int_{u_{17}}^{u_{18}} \frac{ds}{\sqrt{(s-u_{17})^2(u_{18}-s)}} = \xi, \tag{3.47}$$

$$\pm\int_{u}^{u_{17}} \frac{ds}{\sqrt{(u_{17}-s)^2(u_{18}-s)}} = \xi. \tag{3.48}$$

Then we derive the solitary wave solution

$$u_{17,18\pm} = \frac{1}{6}B\left(1-3\tanh^2\left(\frac{1}{2}\sqrt{\frac{1}{2}B}\,\xi\right)\right), \tag{3.49}$$

and the unbounded wave solution

$$u_{19\pm} = \frac{1}{6}B\left(1-3\coth^2\left(\frac{1}{2}\sqrt{\frac{1}{2}B}\,\xi\right)\right). \tag{3.50}$$

(2) When $h = h_2$, there is the special orbit Γ_{13} crossing the points $(u_{19}, 0)$, $(u_{20}, 0)$ and $(u_{21}, 0)$,

$$\Gamma_{13}:\ y = \pm\sqrt{(u-u_{21})(u-u_{20})(u_{19}-u)}, \quad u < u_{19}. \tag{3.51}$$

Substituting (3.51) into (3.2) and integrating along the orbit Γ_{13} yield

$$\pm\int_{u}^{u_{19}} \frac{ds}{\sqrt{(s-u_{21})(s-u_{20})(u_{19}-s)}} = \xi. \tag{3.52}$$

We derive the solution of the periodic breaking wave

$$u_{20\pm} = -\frac{3\sqrt{\Delta}}{2A}\left[1-\csc^2\left(\frac{1}{2}\sqrt{\frac{3}{2A}}\,\Delta^{\frac{1}{4}}\xi\right)\right]+\frac{B+\sqrt{\Delta}}{2A}. \tag{3.53}$$

(3) When $h = 0$, the closed orbit Γ_{14} and special orbit Γ^*_{14} cross the points $(u_{22}, 0)$, $(u_{23}, 0)$, and $(u_{24}, 0)$,

$$\Gamma_{14}:\ y = \pm\sqrt{(u-u_{23})(u-u_{22})(u_{24}-u)}, \quad u_{22} < u_{23} < u < u_{24}, \tag{3.54}$$

$$\Gamma_{14}^{*}:\ y=\pm\sqrt{(u_{22}-u)(u_{23}-u)(u_{24}-u)},\quad u<u_{22}<u_{23}<u_{24}. \tag{3.55}$$

Substituting (3.54) and (3.55) into (3.2) and performing integration independently over the orbits Γ_{14} and Γ_{14}^{*} , respectively, yield

$$\pm\int_{u_{23}}^{u_{24}}\frac{ds}{\sqrt{(s-u_{23})(s-u_{22})(u_{24}-s)}}=\xi, \tag{3.56}$$

$$\pm\int_{u}^{u_{22}}\frac{ds}{\sqrt{(u_{22}-s)(u_{23}-s)(u_{24}-s)}}=\xi. \tag{3.57}$$

We derive the solution of the periodic breaking wave

$$u_{21\pm}=u_{24}+(u_{23}-u_{24})\,\mathrm{sn}^2\left(\frac{\sqrt{u_{24}-u_{22}}}{2}\xi,\ \sqrt{\frac{u_{23}-u_{24}}{u_{22}-u_{24}}}\right), \tag{3.58}$$

and the unbounded wave solution

$$u_{22\pm}=u_{24}+\frac{u_{22}-u_{24}}{\mathrm{sn}^2\left(\frac{\sqrt{u_{24}-u_{22}}}{2}\xi,\ \sqrt{\frac{u_{23}-u_{24}}{u_{22}-u_{24}}}\right)}. \tag{3.59}$$

(4) When $h=-11$, there is the closed orbit Γ_{15} crossing the points $(u_{25},0)$ and $(u_{26},0)$, and special orbit Γ_{15}^{*} crosses the point $(u_{35},0)$,

$$\Gamma_{15}:\ y=\pm\sqrt{(u-u_{26})(u_{27}-u)(u-u_{25})},\quad u_{25}<u_{26}<u<u_{27}, \tag{3.60}$$

$$\Gamma_{15}^{*}:\ y=\pm\sqrt{(u_{26}-u)(u_{27}-u)(u_{25}-u)},\quad u<u_{25}<u_{26}<u_{27}. \tag{3.61}$$

Substituting (3.60) and (3.61) into (3.2) and integrating along the orbits Γ_{15} and Γ_{15}^{*} , respectively, yield

$$\pm\int_{u_{26}}^{u_{27}}\frac{ds}{\sqrt{(s-u_{26})(u_{27}-s)(s-u_{25})}}=\xi, \tag{3.62}$$

$$\pm\int_{u}^{u_{25}}\frac{ds}{\sqrt{(u_{26}-s)(u_{27}-s)(u_{25}-s)}}=\xi. \tag{3.63}$$

Then we obtain the periodic wave solution

$$u_{23\pm}=u_{27}+(u_{26}-u_{27})\,\mathrm{sn}^2\left(\frac{\sqrt{u_{27}-u_{25}}}{2}\xi,\ \sqrt{\frac{u_{26}-u_{27}}{u_{25}-u_{27}}}\right), \tag{3.64}$$

and periodic breaking wave solution

$$u_{24\pm}=u_{27}+\frac{u_{25}-u_{27}}{\mathrm{sn}^2\left(\frac{\sqrt{u_{27}-u_{25}}}{2}\xi,\ \sqrt{\frac{u_{26}-u_{27}}{u_{25}-u_{27}}}\right)}. \tag{3.65}$$

(5) When $h=h_2-0.1$, special orbit Γ_{17} crosses the points $(u_{28},0)$, $(u_{29},0)$, and $(u_{30},0)$,

$$\Gamma_{17}:\ y=\pm\sqrt{(u-u_{29})(u-u_{30})(u_{28}-u)},\quad u<u_{28}. \tag{3.66}$$

Substituting(3.66) into (3.2) and integrating along the orbit Γ_{17} yield

$$\pm \int_{u}^{u_{28}} \frac{ds}{\sqrt{(u_{29}-s)(s-u_{30})(u_{28}-s)}} = \xi. \tag{3.67}$$

We get the periodic breaking wave solution

$$u_{25\pm} = -\frac{3\sqrt{\Delta}}{2A}\left[1-\csc^{2}\left(\frac{1}{2}\sqrt{\frac{3}{2A}}\Delta^{\frac{1}{4}}\xi\right)\right] + \frac{B+\sqrt{\Delta}}{2A}. \tag{3.68}$$

4. Physical interpretation

In this section, we provide an interpretation of the figures corresponding to the derived exact solutions. For Figures 2 and 3 we select parameters $A = -2$, $B = -6$, $k = 1$, $l = 1$, $m = 1$, $c = 2$, $y = 0$, $z = 0$, and $h = h_1 = 0$. They represent multi-peaked bright soliton solutions and a solution corresponding to an unbounded wave. For Figures 4 and 5, we select parameters $A = -2$, $B = -6$, $k = 1$, $l = 1$, $m = 1$, $c = 2$, $y = 0$, $z = 0$, and $h = -4.5$. They characterize solutions of the periodic wave-type and periodic solutions of the breaking wave-type. For Figures 6 and 7 we select parameters $A = -2$, $B = -6$, $k = 1$, $l = 1$, $m = 1$, $c = 2$, $y = 0$, $z = 0$, and $h = h_1$. They stand for solutions of a dark-soliton and solutions of unbounded wave-type. For Figures 8 and 9, we select parameters $A = -2$, $B = -6$, $k = 1$, $l = 1$, $m = 1$, $c = 2$, $y = 0$, $z = 0$, and $h = -9$. They represent a wave with periodicity and periodic breaking wave-type solutions. For Figures 10 and 11, we select parameters $A = -2$, $B = -6$, $k = 1$, $l = 1$, $m = 1$, $c = 2$, $y = 0$, $z = 0$, and $h = h_1$. They stand for multiple dark-soliton solutions and a solution of unbounded wave-type. For Figures 12 and 13, we select parameters $A = -2$, $B = -6$, $k = 1$, $l = 1$, $m = 1$, $c = 2$, $y = 0$, $z = 0$, and $h = 0$. They characterize the solution of the periodic breaking wave-type and unbounded wave-type solution.

Periodic wave-type, periodic breaking wave-type, solitary wave-type, and unbounded wave-type solutions can help us understand the dynamics of nonlinear waves in fluid mechanics and characterize the real three-dimensional wave behaviors of bubbly fluids. The relevant research covers complex problems across fluid physics, nonlinear optics, biology, and economics, and provides theoretical references for investigations in various disciplines.

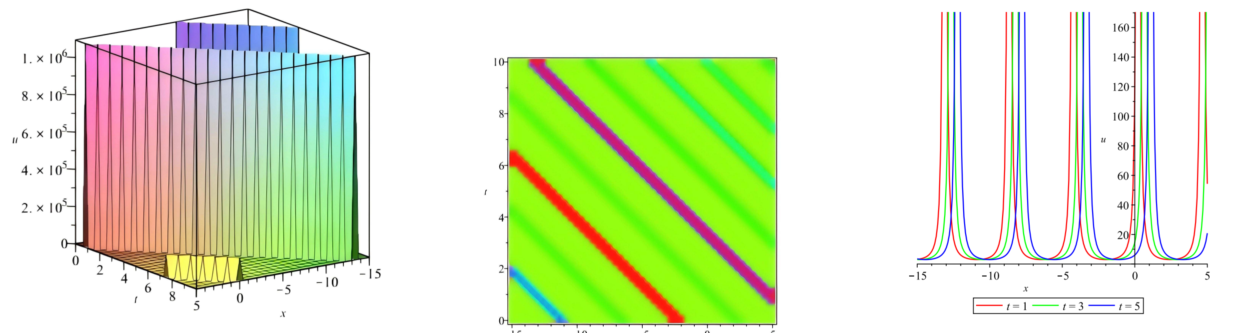

(a) A surface plot in three dimensions

(b) A plot of density distribution

(c) A function curve plot in two dimensions

Figure 2. multi-peaked bright soliton solution $u_{1,2\pm}$ of (3.7), for $A = -2$, $B = -6$, $k = 1$, $l = 1$, $m = 1$, $c = 2$, $y = 0$, $z = 0$, $h = h_1$.

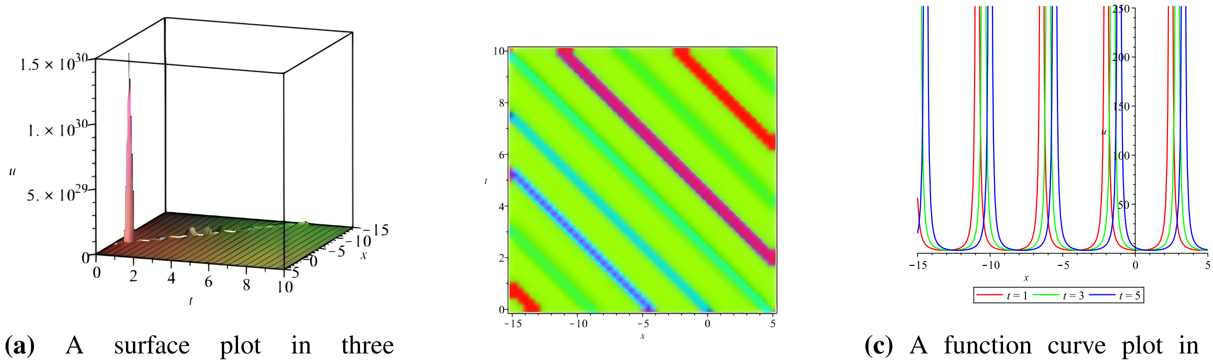

(a) A surface plot in three dimensions

(b) A plot of density distribution

(c) A function curve plot in two dimensions

Figure 3. a solution of an unbounded wave $u_{3\pm}$ of (3.8) for $A = -2$, $B = -6$, $k = 1$, $l = 1$, $m = 1$, $c = 2$, $y = 0$, $z = 0$, $h = h_1$.

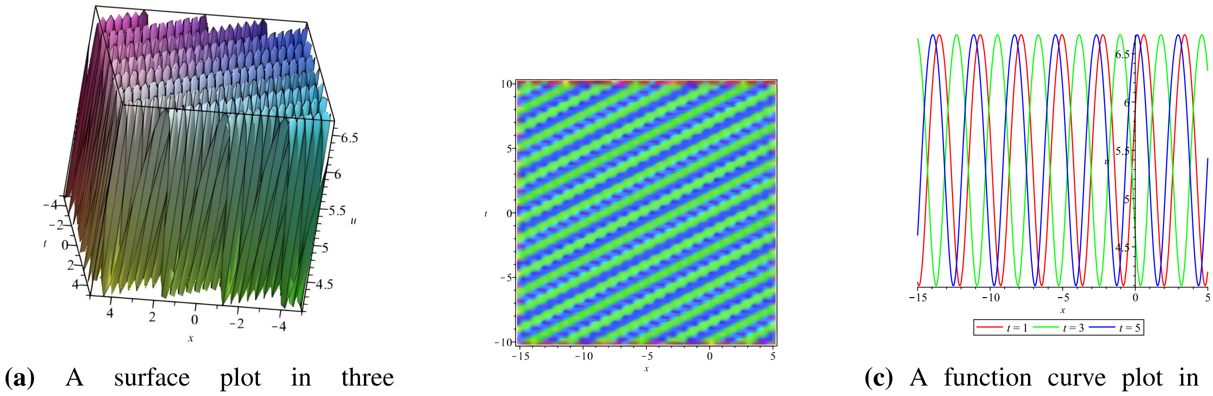

(a) A surface plot in three dimensions

(b) A plot of density distribution

(c) A function curve plot in two dimensions

Figure 4. Solutions of periodic wave-type $u_{5\pm}$ of (3.16) for $A = -2$, $B = -6$, $C = 0$, $k = 1$, $l = 1$, $m = 1$, $c = 2$, $y = 0$, $z = 0$, and $h = -4.5$.

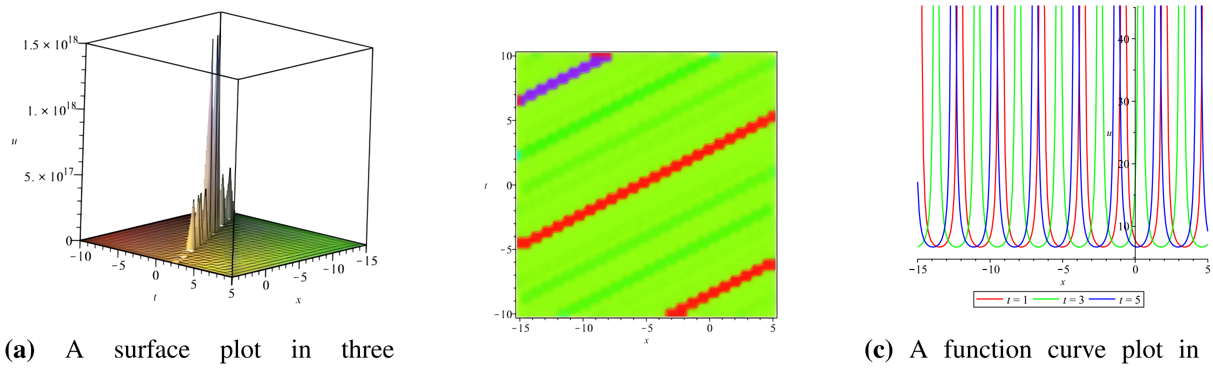

(a) A surface plot in three dimensions

(b) A plot of density distribution

(c) A function curve plot in two dimensions

Figure 5. Periodic solutions of breaking wave-type $u_{6\pm}$ of (3.17) for $A = -2$, $B = -6$, $C = 0$, $k = 1$, $l = 1$, $m = 1$, $c = 2$, $y = 0$, $z = 0$, and $h = -4.5$.

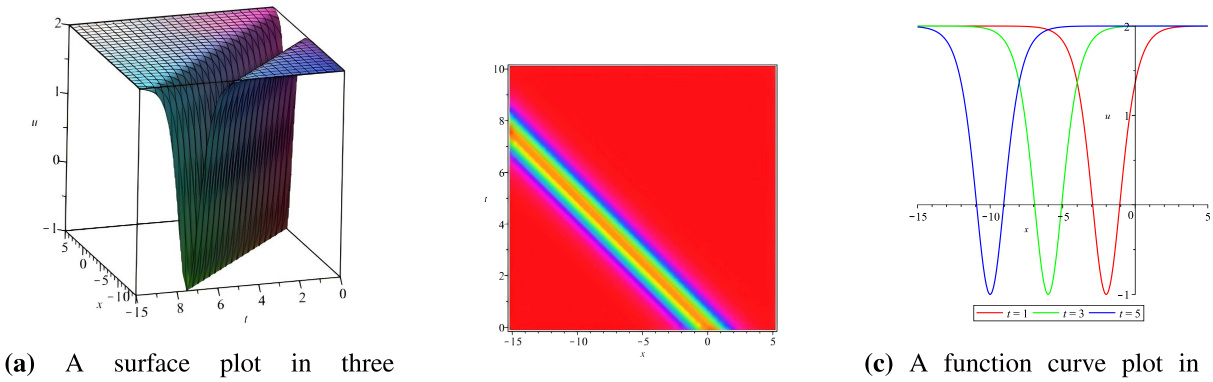

(a) A surface plot in three dimensions

(b) A plot of density distribution

(c) A function curve plot in two dimensions

Figure 6. Solutions of a dark-soliton $u_{8,9\pm}$ of (3.25), for $A = -2$, $B = -6$, $C = 0.5$, $k = 1$, $l = 1$, $m = 1$, $c = 2$, $y = 0$, $z = 0$, and $h = h_1$.

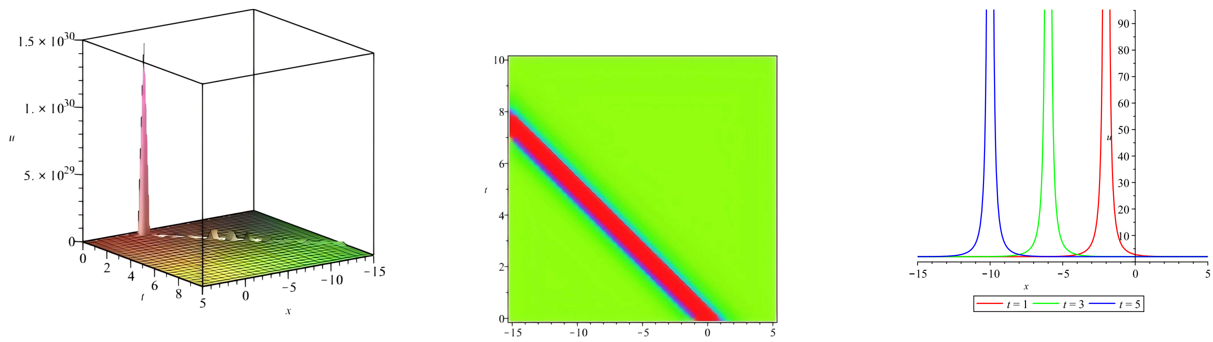

(a) A surface plot in three dimensions

(b) A plot of density distribution

(c) A function curve plot in two dimensions

Figure 7. Solution of unbounded wave-type $u_{10\pm}$ of (3.26), for $A = -2$, $B = -6$, $C = 0.5$, $k = 1$, $l = 1$, $m = 1$, $c = 2$, $y = 0$, $z = 0$, and $h = h_1$.

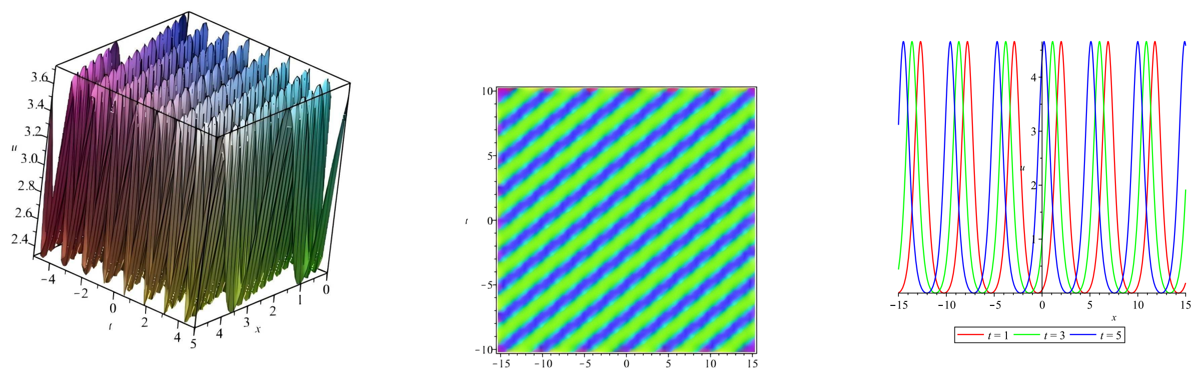

(a) A surface plot in three dimensions

(b) A plot of density distribution

(c) A function curve plot in two dimensions

Figure 8. A wave with periodicity $u_{14\pm}$ to (3.40), for $A = -2$, $B = -6$, $C = 0.5$, $k = 1$, $l = 1$, $m = 1$, $c = 2$, $y = 0$, $z = 0$, $h = -9$.

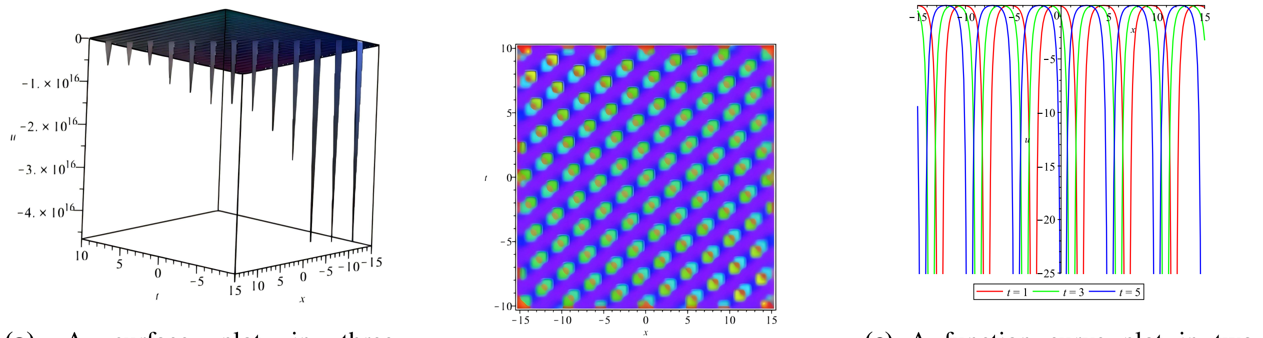

(a) A surface plot in three dimensions

(b) A plot of density distribution

(c) A function curve plot in two dimensions

Figure 9. Periodic breaking wave-type solutions $u_{15\pm}$ of (3.41), for $A = -2$, $B = -6$, $C = 0.5$, $l = 1$, $m = 1$, $c = 2$, $y = 0$, $z = 0$, and $h = -9$.

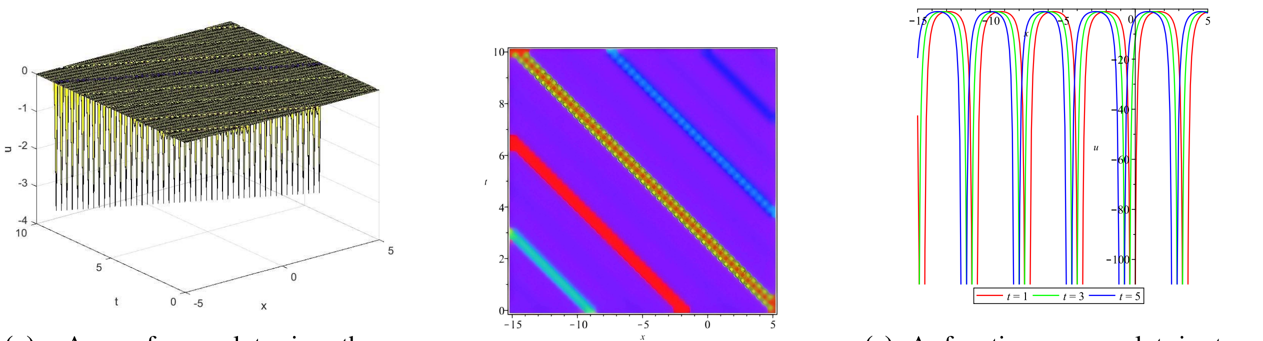

(a) A surface plot in three dimensions

(b) A plot of density distribution

(c) A function curve plot in two dimensions

Figure 10. Multiple dark-soliton solutions $u_{17,18\pm}$ of (3.49), for $A = -2$, $B = -6$, $C = 4.5$, $k = 1$, $l = 1$, $m = 1$, $c = 2$, $y = 0$, $z = 0$, and $h = h_1$.

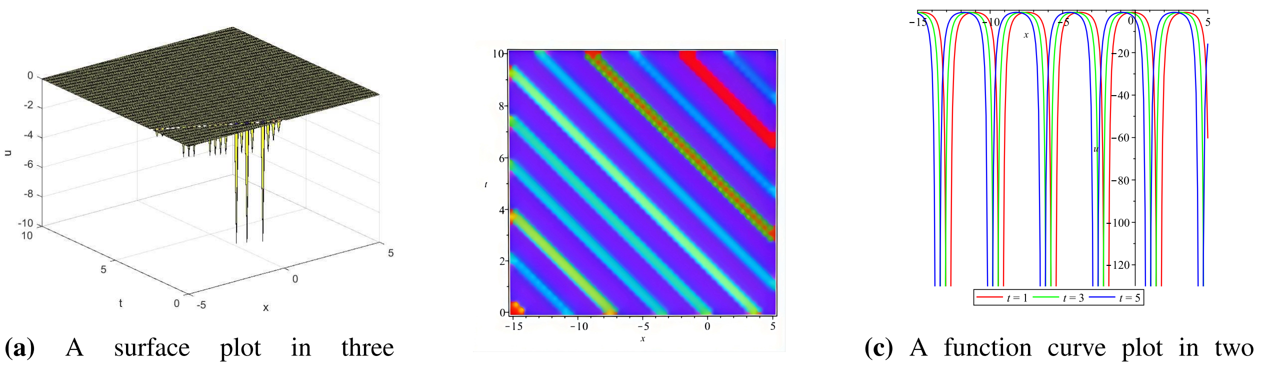

(a) A surface plot in three dimensions

(b) A plot of density distribution

(c) A function curve plot in two dimensions

Figure 11. Solution of unbounded wave-type $u_{19\pm}$ to (3.50), for $A = -2$, $B = -6$, $C = 4.5$, $k = 1$, $l = 1$, $m = 1$, $c = 2$, $y = 0$, $z = 0$, and $h = h_1$.

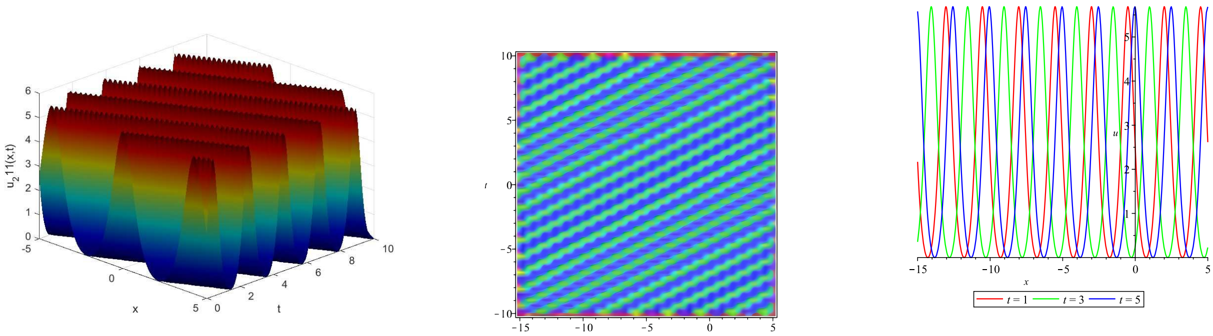

(a) A surface plot in three dimensions

(b) A plot of density distribution

(c) A function curve plot in two dimensions

Figure 12. Solution of periodic breaking wave-type $u_{21\pm}$ of (3.58), for $A = -2$, $B = -6$, $C = 4.5$, $k = 1$, $l = 1$, $m = 1$, $c = 2$, $y = 0$, $z = 0$, $h = 0$.

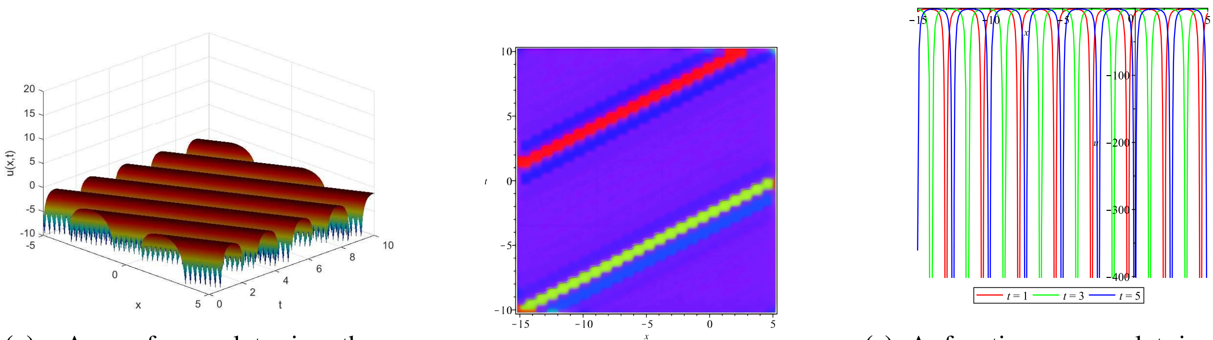

(a) A surface plot in three dimensions

(b) A plot of density distribution

(c) A function curve plot in two dimensions

Figure 13. Unbounded wave-type solution $u_{22\pm}$ of (3.59), for $A = -2$, $B = -6$, $C = 4.5$, $k = 1$, $l = 1$, $m = 1$, $c = 2$, $y = 0$, $z = 0$, and $h = 0$.

5. Sensitivity analysis

Sensitivity analysis is a pivotal tool for understanding the response of dynamical systems to parameter variations. This type of analysis reveals the influence of specific parameters on system behaviors and provides profound insights into stability and control. In particularly complex systems, even small parameter variations may lead to significant changes in dynamics. In this part, the Runge-Kutta algorithm is adopted to observe the sensitivity with respect to the specified dynamical system in the equation.

The parameters are specified as follows: $A = 2$, $B = 6$, $C = 0.5$, $k = 1$, $l = 1$, $m = 1$, $c = 1$, and $n = 1$. Under the given initial conditions, there exist two equilibrium points for the dynamical system. We have two equilibrium points, $u_{01} = 3.0811$ and $u_{02} = -0.0811$, along with sensitivity coefficients. These include the sensitivities of the equilibrium point u_{01} with respect to parameters A, B, and C: $\frac{\partial u_{01}}{\partial A} = -0.00104$, $\frac{\partial u_{01}}{\partial B} = -0.01283$, and $\frac{\partial u_{01}}{\partial C} = -0.15811$, respectively, and the sensitivities of the equilibrium point u_{02} with respect to parameters A, B, and C: $\frac{\partial u_{02}}{\partial A} = 1.50105$, $\frac{\partial u_{02}}{\partial B} = -0.48717$, and $\frac{\partial u_{02}}{\partial C} = 0.15811$, respectively.

Figure 14 shows the baseline trajectory plots, presenting nonlinear periodic oscillations, which represent the natural evolution of the state variable u under no parameter perturbations and serve as the reference frame for the sensitivity analysis. a exhibits periodic oscillations that are phase-complementary to those in b.

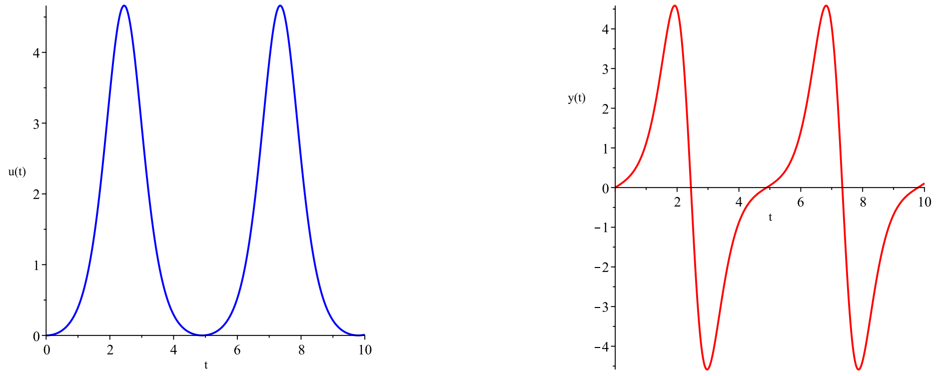

(a) $u(t)$ baseline trajectory **(b)** $y(t)$ baseline trajectory

Figure 14. Baseline trajectories of the solutions with $t = 0 : 0.01 : 10$, $A = -2$, $B = -6$, $C = 0.5$, $u(0) = 0$, and $y(0) = 0$.

In Figure 15, we solve for $u(t)$ via the RK4 method, where the time domain is $t \in [0, 10]$ with a step size of 0.01, and the conditions that specify the initial state are $u(0) = 0$ and $y(0) = 0$. Figure 15 presents the sensitivity analysis with respect to parameter A. In the positive interval, an increase in A leads to an increase in the equilibrium point; in the negative interval, an increase in A conversely leads to a decrease in the point that satisfies the equilibrium condition. The point that satisfies the equilibrium condition is sensitive to parameter A at a peak time: Even a small perturbation in A can cause a significant change in the equilibrium point; for example, a variation of 0.01 in parameter A induces a shift of 0.5 in the equilibrium point.

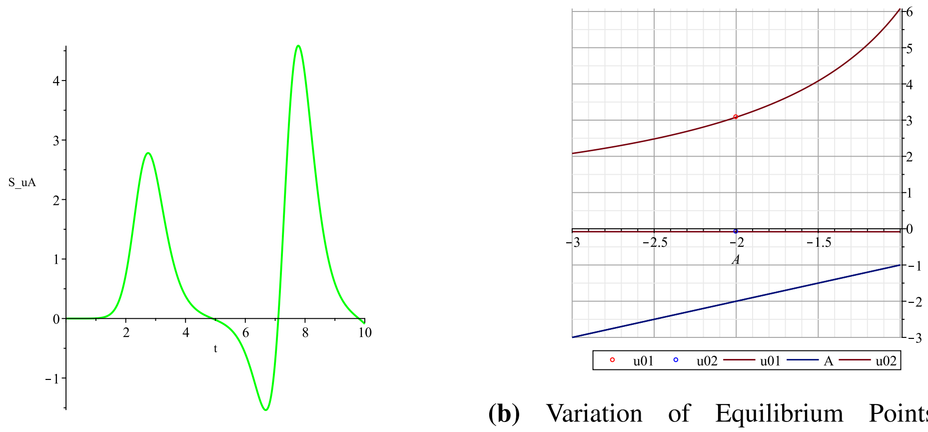

(a) Sensitivity of u to A **(b)** Variation of Equilibrium Points with Parameter A

Figure 15. (a) Fix $B = -6$, and $C = 0.5$ unchanged; perturb parameter A to $A = -2 + 0.01 = -1.99$. (b) Curves of equilibrium solutions u vary for A when $B = -6$ and $C = 0.5$ are fixed.

In Figure 16, we solve for $u(t)$ by means of the RK4 method. The domain of the temporal evolution is $t \in [0, 10]$ with a step size for $h = 0.01$, as well as initial state specifications $u(0) = 0$ and $y(0) = 0$. Figure 16 presents the sensitivity analysis with respect to parameter B. The influence of B on the equilibrium point is generally weak: Even at the peak time, a variation of 0.01 in parameter B induces a shift of 0.02 in the equilibrium point. The alternation between positive and negative intervals is not obvious, which further verifies that the sensitivity of the equilibrium point position to parameter B is very small. Therefore, parameter B mainly serves to fine-tune the position of the equilibrium point.

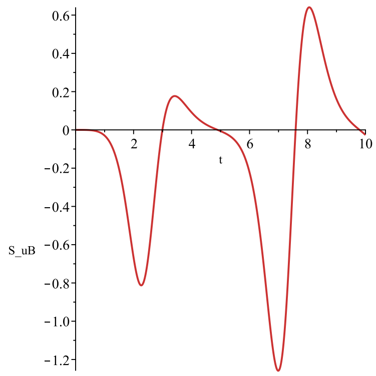

(a) Sensitivity of u to B

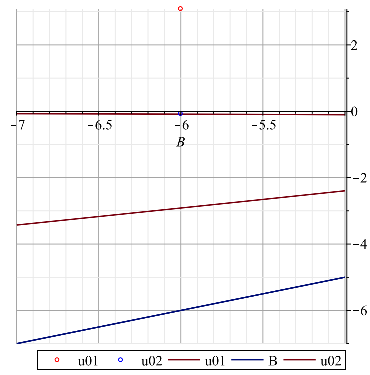

(b) Variation of Equilibrium Points with Parameter B

Figure 16. (a) Fix $A = -2$, and $C = 0.5$ is unchanged; perturb parameter B to $B = -6+0.01 = -5.99$. (b) The curves of the equilibrium solution u vary with B when $A = -2$ and $C = 0.5$ are fixed.

In Figure 17, we solve for $u(t)$ using the RK4 method. The time domain is $t \in [0, 10]$ with a step size of $h = 0.01$, along with the starting values of $u(0) = 0$ and $y(0) = 0$. Figure 17 presents the sensitivity analysis with respect to parameter C. For example, a variation of 0.01 in parameter C induces a shift of 1.0 in the equilibrium point, which is twice that of A and five times that of B. At the peak time ($t \approx 8$), the system reaches its most vulnerable point: A tiny error in C at this moment will deviate from the baseline trajectory, further verifying that parameter C is the most sensitive parameter for controlling the equilibrium point position.

We also conduct a sensitivity analysis of the orbital energy. There exist two Hamiltonian energy values, $h_{01} = -10.0205$ and $h_{02} = 0.0205$. The sensitivity coefficients of each parameter are presented in Table 1.

Table 1 reveals that parameter C exerts the strongest influence on h_{01}, significantly outweighing the effects of B and A. While C also affects h_{02} to some extent, parameter A dominates the sensitivity of h_{02}, acting as the key parameter for tuning homoclinic orbital energy and solitary wave amplitude. Overall, A is highly sensitive to the energy of the equilibrium near 0, C strongly influences the energy of the equilibrium far from 0, and B exhibits the weakest effect.

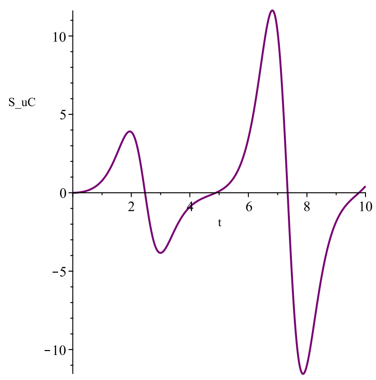

(a) Sensitivity of u to C

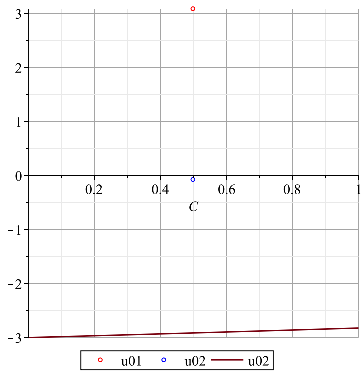

(b) Variation of Equilibrium Points with Parameter C

Figure 17. (a) Fix $A = -2$, and $B = -6$ is unchanged; perturb parameter C to $C = 0.5+0.01 = 0.51$. (b) The curves of the equilibrium solution u vary with C when $A = -2$ and $B = -6$ are fixed.

Figure 18 illustrates the influence of parameter A on the morphology of the homoclinic orbit. Combined with the effect of parameter A on the equilibrium point position, it can be demonstrated that although parameter A exerts a strong influence on the morphology of the homoclinic orbit, its sensitivity to the equilibrium point position is extremely low.

Table 1. Sensitivity analysis of energy with respect to parameters A, B, and C.

Energy value	Sensitivity to A	Sensitivity to B	Sensitivity to C
$h_{01} = -10.0205$	0.00017805942	0.003291754872	0.08113883050
$h_{02} = 0.0205$	−9.750178045	4.746708247	−3.081138830

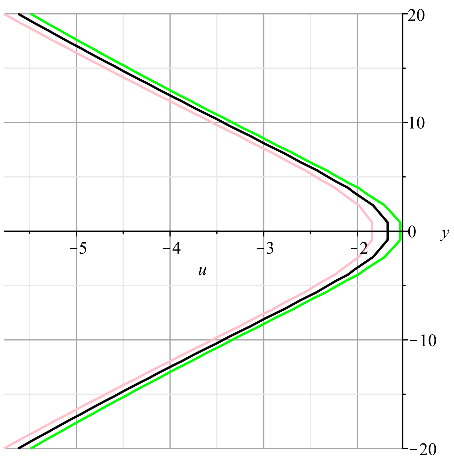

Figure 18. The effect of parameter A on orbital morphology with fixed $B = -6$, and $C = 0.5$. The values $A = -2.2, -2$, and -1.8, correspond to the green, black, and pink curves, respectively.

6. Quasi periodic and chaotic dynamics

Periodic perturbations are ubiquitous in various systems, exerting pronounced influences on system dynamics and inducing chaotic motions. In this section, we investigate the dynamical behaviors of the system under periodic perturbations to reveal how slight variations in perturbations can trigger drastic changes in the system's dynamical properties.

We introduce the periodic perturbation term $\varepsilon\sin(\varpi t)$ to explore the periodic behaviors of the system,

$$\begin{cases} \dfrac{du}{d\xi} = y, \\ \dfrac{dy}{d\xi} = Au^2 - Bu + C + \varepsilon\sin(\varpi t), \end{cases} \tag{6.1}$$

where ε denotes the external amplitude and ϖ represents the excitation frequency. When analyzing the evolutionary law of system (6.1) with respect to variations in perturbation amplitude and frequency, we fix the system parameters A, B, and C with $A = -2$, $B = -6$, and $C = 4.5$. The periodic and quasi-periodic dynamical characteristics of the system are characterized via two-dimensional and three-dimensional diagrams.

For fixed parameters $A = -2$, $B = -6$, and $C = 4.5$, we select the initial conditions $\varepsilon = 0$ and $\varpi = 0$, as shown in Figure 19. Without the excitation of external periodic forces, the curve exhibits perfect periodicity. To examine the influence induced by external periodic forces, we set $\varepsilon = 0.19$ and $\varpi = 0.04$, and $\varepsilon = 1.25$ and $\varpi = 1.24$, corresponding to Figures 20 and 21, respectively. As the external periodic force intensifies, the irregularity of the wave period gradually increases.

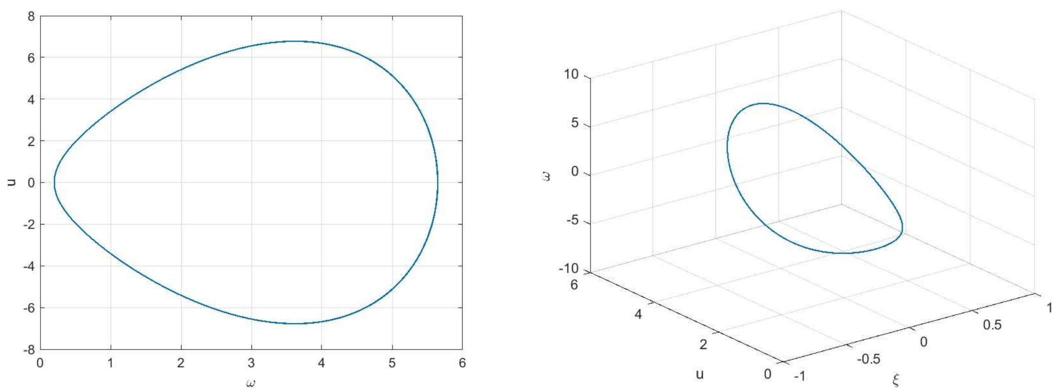

Figure 19. Phase portraits of system (6.1) $A = -2$, $B = -6$, $C = 4.5$, $\varepsilon = 0$, and $\varpi = 0$.

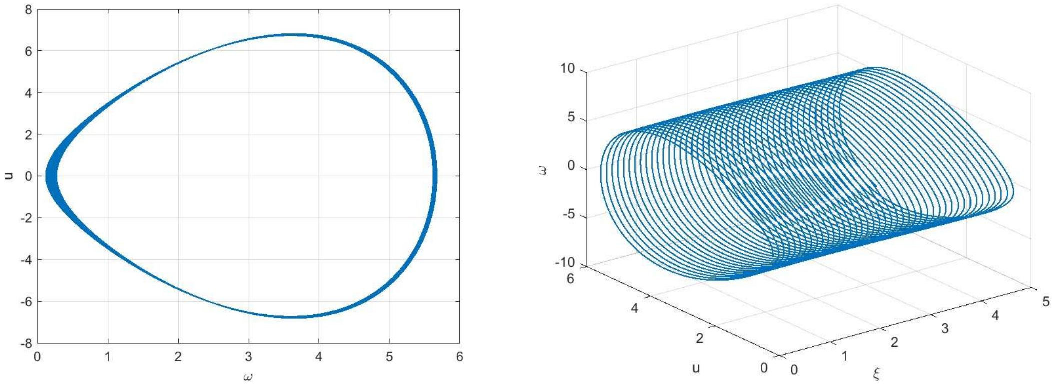

Figure 20. Phase portraits of system (6.1) $A = -2$, $B = -6$, $C = 4.5$, $\varepsilon = 0.19$, and $\varpi = 0.04$.

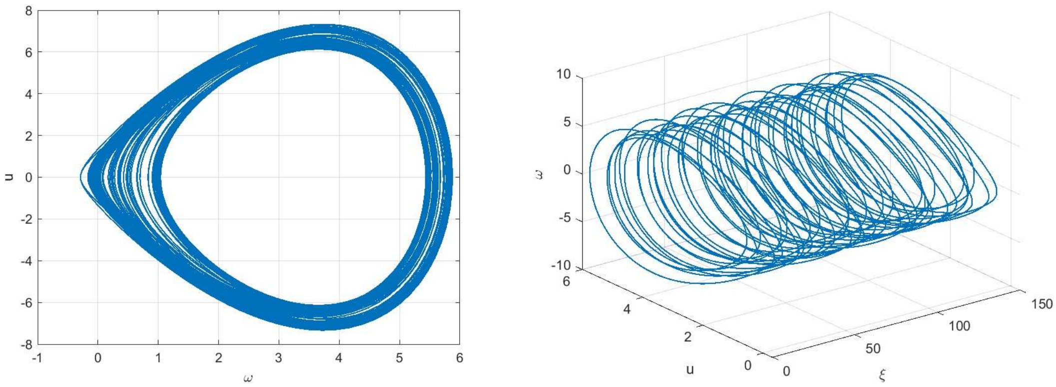

Figure 21. Phase portraits of system (6.1) $A = -2$, $B = -6$, $C = 4.5$, $\varepsilon = 1.25$, and $\varpi = 1.24$.

As shown in Figure 22, the largest Lyapunov exponent converges to a positive value while the second Lyapunov exponent remains negative, which numerically verifies the chaotic property of system (6.1).

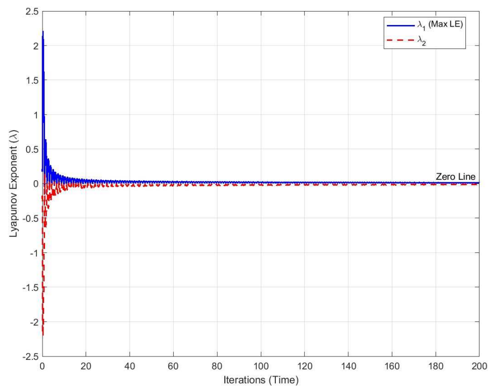

(a) $\varepsilon = 0.2$, $\varpi = 1.4$

Figure 22. Convergence plot for the Lyapunov exponent for system (6.1), $A = -2$, $B = -6$, $C = 4.5$.

7. Conclusions

In this work, we study the three spatial dimensions and one time dimension nonlinear PDE governing wave propagation in a gas-bubble-containing liquid. Focusing on bifurcation behavior for an associated dynamical system, we derive phase portraits for a dynamical system. Under appropriate parameter selections, we derive exact solutions from the obtained phase portraits, including solutions of a periodic wave, wave solution of unboundedness, solutions of a periodic breaking wave, and solutions in the form of solitary waves. Since some solutions possess significant physical significance, it is necessary to explore their dynamic behaviors. To reveal the dynamical behaviors of these solutions, we select appropriate parameter values to plot the three-dimensional spatial evolution surfaces, two-dimensional density contours, and multi-time slice diagrams for each solution. In addition, we conduct an analysis of the sensitivity of the system under small perturbations to further investigate the stability of the solutions. The system exhibits chaotic dynamics under external periodic forcing, and the chaotic behavior of the system is further verified by Lyapunov exponents. This reveals that special attention should be given to external periodic excitations and small disturbances in realistic applications. The results of this research offer an important theory foundation to study the numerical solutions of the model by using the numerical simulations methods in [49–51].

Nevertheless, bifurcation analysis of dynamical systems is not applicable to all equations. This method cannot be adopted for equations that fail to yield the corresponding dynamical systems. Furthermore, for equations with high-order nonlinear terms, the bifurcation phase portraits of their associated dynamical systems are highly complicated, which brings difficulties to theoretical analysis. In addition, standard bifurcation analysis is invalid for Hamiltonian systems containing singular points. Accordingly, research entailing the above limitations should be carried out in future work.

Author contributions

Miaomiao Li: Writing - original draft, Methodology. Zenggui Wang: Conceptualization, Methodology, Validation, Supervision, Writing - review & editing. All authors have read and approved the final version of the manuscript for publication.

Use of Generative-AI tools declaration

The authors declares they have not used Artificial Intelligence (AI) tools in the creation of this article.

Acknowledgements

This work was supported by Natural Science Foundation of Shandong Province (Grant ZR2026MS0004,ZR2021MA084).

Conflicts of interest

The authors, who participate in this research, declare that they have no competing interests in financial matters or connections of a personal nature that might have affected the study outcomes.

References

1. F. Zhang, X. P. Xin, P. F. Han, Y. Zhang, $\bar{\partial}$-dressing approach and N-soliton solutions of the general reverse-space nonlocal nonlinear schrödinger equation, *Appl. Math. Lett.*, **160** (2025), 109293. https://doi.org/10.1016/j.aml.2024.109293
2. H. L. Qiao, A. J. Cheng, A fast modified finite difference method for time fractional diffusion equations with weakly singular solution, *J. Appl. Math. Comput.*, **70** (2024), 3631–3660. https://doi.org/10.1007/s12190-024-02110-7
3. S. S. Xia, Z. G. Wang, The cauchy problem of dissipative hyperbolic mean curvature flow, *Math. Methods Appl. Sci.*, **47** (2024), 9409–9421. https://doi.org/10.1002/mma.10076
4. S. Ibrahim, Optical soliton solutions for the nonlinear third-order partial differential equation, *Adv. Differ. Equ. Control Process.*, **29** (2022), 127–138. https://doi.org/10.17654/0974324322037
5. Z. G. Wang, S. X. Lv, B. Zhao, Dissipative hyperbolic mean curvature flow for closed convex plane curves, *J. Funct. Anal.*, **285** (2023), 110023. https://doi.org/10.1016/j.jfa.2023.110023
6. N. A. Kudryashov, D. I. Sinelshchikov, Equation for the three-dimensional nonlinear waves in liquid with gas bubbles, *Phys. Scr.*, **85** (2012), 25402. https://doi.org/10.1088/0031-8949/85/02/025402
7. G. F. Deng, Y. T. Gao, Integrability, solitons, periodic and travelling waves of a generalized (3+1)-dimensional variable-coefficient nonlinear-wave equation in liquid with gas bubbles, *Eur. Phys. J. Plus*, **132** (2017), 255. https://doi.org/10.1140/epjp/i2017-11515-8
8. M. Wang, B. Tian, Y. Sun, Z. Zhang, Lump, mixed lump-stripe and rogue wave-stripe solutions of a (3+1)-dimensional nonlinear wave equation for a liquid with gas bubbles, *Comput. Math. Appl.*, **79** (2020), 576–587. https://doi.org/10.1016/j.camwa.2019.07.006
9. W. H. Liu, Y. F. Zhang, Resonant multiple wave solutions, complexiton solutions and rogue waves of a generalized (3+1)-dimensional nonlinear wave in liquid with gas bubbles, *Waves Random Complex Media*, **30** (2020), 470–480. https://doi.org/10.1080/17455030.2018.1528026
10. M. M. Awad, A. A. Elsadany, M. K. Elboree, Multiple rogue waves solutions for a (3+1)-dimensional nonlinear wave in liquid with gas bubbles via hirota bilinear equation method, *Examples Counterexamples*, **8** (2025), 100202. https://doi.org/10.1016/j.exco.2025.100202
11. A. S. Khalifa, N. M. Badra, H. M. Ahmed, W. B. Rabie, H. Emadifar, K. K. Ahmed, Building novel solitary wave solutions for the generalized non-linear (3+1)-dimensional wave equation with gas bubbles in fluids using an analytic method, *Partial Differ. Equ. Appl. Math.*, **16** (2025), 101272. https://doi.org/10.1016/j.padiff.2025.101272
12. T. A. Min, M. G. Hafez, S. Akther, Dynamical analysis and exact solitary wave solutions of a (3+1)-dimensional davey-stewartson system with parabolic law nonlinearity, *AIP Adv.*, **16** (2026), 015211. https://doi.org/10.1063/5.0306625

13. Y. R. Hu, F. Zhang, X. P. Xin, Lie symmetry analysis, optimal system and exact solutions of variable-coefficients sakovich equation, *J. Geom. Phys.*, **184** (2023), 104712. https://doi.org/10.1016/j.geomphys.2022.104712

14. E. M. Almetwally, R. Saleh, S. M. Mabrouk, A. S. Rashed, Analysis of gas bubbling dynamics via lie symmetry approach of nonlinear wave equation, *Sci. Rep.*, **15** (2025), 29179. https://doi.org/10.1038/s41598-025-09588-6

15. M. L. Wang, Y. B. B. Zhou, Z. Li, Application of a homogeneous balance method to exact solutions of nonlinear equations in mathematical physics, *Phys. Lett. A*, **216** (1996), 67–75. https://doi.org/10.1016/0375-9601(96)00283-6

16. M. L. Wang, Solitary wave solutions for variant boussinesq equations, *Phys. Lett. A*, **199** (1995), 169–172. https://doi.org/10.1016/0375-9601(95)00092-h

17. Y. R. Hu, F. Zhang, X. P. Xin, H. Z. Liu, Darboux transformation and exact solutions of the variable coefficient nonlocal newell-whitehead equation, *Bull. Malays. Math. Sci. Soc.*, **45** (2022), 1811–1822. https://doi.org/10.1007/s40840-022-01285-1

18. C. Wang, Y. Shi, W. A. Yang, X. P. Xin, Darboux transformations and exact solutions of nonlocal kaup-newell equations with variable coefficients, *Appl. Math. Lett.*, **163** (2025), 109456. https://doi.org/10.1016/j.aml.2025.109456

19. J. H. He, X. H. Wu, Exp-function method for nonlinear wave equations, *Chaos, Soliton. Fract.*, **30** (2006), 700–708. https://doi.org/10.1016/j.chaos.2006.03.020

20. S. D. Zhu, The generalizing Riccati equation mapping method in non-linear evolution equation: application to (2+1)-dimensional Boiti-Leo-Pempinelle equation, *Chaos, Soliton. Fract.*, **37** (2008), 1335–1342. https://doi.org/10.1016/j.chaos.2006.10.015

21. M. K. Elboree, The jacobi elliptic function method and its application for two component bkp hierarchy equations, *Comput. Math. Appl.*, **62** (2011), 4402–4414. https://doi.org/10.1016/j.camwa.2011.10.015

22. E. C. Aslan, M. Inc, Optical solitons and rogue wave solutions of NLSE with variables coefficients and modulation instability analysis, *Comput. Methods Differ. Equ.*, **10** (2022), 905–913. https://doi.org/10.22034/cmde.2021.36045.1624

23. B. Ren, Symmetry reduction related with nonlocal symmetry for gardner equation, *Commun. Nonlinear Sci. Numer. Simul.*, **42** (2017), 456–463. https://doi.org/10.1016/j.cnsns.2016.06.017

24. B. Kalegowda, R. Rangarajan, Multi-soliton solutions to the generalized Boussinesq equation of tenth order, *Comput. Methods Differ. Equ.*, **11** (2023), 727–737. https://doi.org/10.22034/cmde.2023.55261.2297

25. K. Karam Ali, R. I. Nuruddeen, A. Yildirim, On the new extensions to the benjamin-ono equation, *Comput. Methods Differ. Equ.*, **8** (2020), 424–445. https://doi.org/10.22034/cmde.2020.32382.1505

26. J. W. Yu, F. J. Yu, Non-autonomous soliton, wave propagation and collision dynamic for (2+1)-dimensional higher-order nonlinear Schrödinger equation with variable coefficients, *Appl. Math. Lett.*, **174** (2026), 109827. https://doi.org/10.1016/j.aml.2025.109827

27. M. X. Zhou, F. J. Yu, Space-time shifted solitons and solution interactions for a generalized nonlocal nonlinear schrödinger equation, *Appl. Math. Lett.*, **178** (2026), 109937. https://doi.org/10.1016/j.aml.2026.109937
28. K. J. Wang, Dynamics of complexiton, Y-type soliton and interaction solutions to the (3+1)-dimensional Kudryashov-Sinelshchikov equation in liquid with gas bubbles, *Results Phys.*, **54** (2023), 107068. https://doi.org/10.1016/j.rinp.2023.107068
29. M. Jin, J. J. Yang, J. Z. Liu, X. P. Xin, The lie symmetry analysis, optimal system, exact solutions and conservation laws of the (2+1)-dimensional variable coefficient disersive long wave equations, *J. Appl. Anal. Comput.*, **13** (2023), 3535–3557. https://doi.org/10.11948/20230147
30. X. P. Xin, M. Jin, J. J. Yang, Y. R. Xia, Nonlocal symmetries and solutions of the (2+1) dimension integrable Burgers equation, *Appl. Math. Lett.*, **148** (2024), 108867. https://doi.org/10.1016/j.aml.2023.108867
31. N. A. Kudryashov, D. I. Sinelshchikov, Equation for the three-dimensional nonlinear waves in liquid with gas bubbles, *Phys. Scr.*, **85** (2012), 025402. https://doi.org/10.1088/0031-8949/85/02/025402
32. S. Yadav, R. Arora, Lie symmetry analysis, optimal system and invariant solutions of (3+1)-dimensional nonlinear wave equation in liquid with gas bubbles, *Eur. Phys. J. Plus*, **136** (2021), 172. https://doi.org/10.1140/epjp/s13360-021-01073-z
33. J. G. Liu, W. H. Zhu, Y. He, Y. K. Wu, Interaction phenomena between lump and solitary wave of a generalized (3+1)-dimensional variable-coefficient nonlinear-wave equation in liquid with gas bubbles, *Commun. Theor. Phys.*, **72** (2020), 085002. https://doi.org/10.1088/1572-9494/ab7709
34. Y. L. Shen, R. X. Yao, Y. Li, New bilinear bäcklund transformation and higher order rogue waves with controllable center of a generalized (3+1)-dimensional nonlinear wave equation, *Commun. Theor. Phys.*, **71** (2019), 161. https://doi.org/10.1088/0253-6102/71/2/161
35. H. Wang, S. F. Tian, T. T. Zhang, Y. Chen, Lump wave and hybrid solutions of a generalized (3+1)-dimensional nonlinear wave equation in liquid with gas bubbles, *Front. Math. China*, **14** (2019), 631–643. https://doi.org/10.1007/s11464-019-0775-7
36. E. M. Almetwally, R. Saleh, S. M. Mabrouk, A. S. Rashed, Analysis of gas bubbling dynamics via lie symmetry approach of nonlinear wave equation, *Sci. Rep.*, **15** (2025), 29179. https://doi.org/10.1038/s41598-025-09588-6
37. O. D. Adeyemo, C. M. Khalique, Lie group theory, stability analysis with dispersion property, new soliton solutions and conserved quantities of 3d generalized nonlinear wave equation in liquid containing gas bubbles with applications in mechanics of fluids, biomedical sciences and cell biology, *Commun. Nonlinear Sci. Numer. Simul.*, **123** (2023), 107261. https://doi.org/10.1016/j.cnsns.2023.107261
38. S. Kumar, I. Hamid, M. A. Abdou, Specific wave profiles and closed-form soliton solutions for generalized nonlinear wave equation in (3+1)-dimensions with gas bubbles in hydrodynamics and fluids, *J. Ocean Eng. Sci.*, **8** (2023), 91–102. https://doi.org/10.1016/j.joes.2021.12.003
39. F. Alizadeh, K. Hosseini, S. Sirisubtawee, E. Hincal, Classical and nonclassical lie symmetries, bifurcation analysis, and jacobi elliptic function solutions to a 3d-modified nonlinear wave equation in liquid involving gas bubbles, *Bound. Value Probl.*, **2024** (2024), 111. https://doi.org/10.1186/s13661-024-01921-8

40. A. M. Wazwaz, W. Alhejaili, S. A. El-Tantawy, Study on extensions of (modified) korteweg-de vries equations: Painlevé integrability and multiple soliton solutions in fluid mediums, *Phys. Fluids*, **35** (2023), 093110. https://doi.org/10.1063/5.0169733
41. H. Z. Liu, A. Yusupu, Dynamical analysis and explicit traveling wave solutions to the higher-dimensional generalized nonlinear wave system, *J. Comput. Appl. Math.*, **445** (2024), 115825. https://doi.org/10.1016/j.cam.2024.115825
42. Y. Z. Ma, Z. G. Wang, Traveling wave solutions, power series solutions and conservation laws of the nonlinear dispersion equation, *J. Appl. Anal. Comput.*, **13** (2023), 2267–2282. https://doi.org/10.11948/20220470
43. M. E. Elbrolosy, A. A. Elmandouh, Bifurcation and new traveling wave solutions for (2+1)-dimensional nonlinear Nizhnik-Novikov-Veselov dynamical equation, *Eur. Phys. J. Plus*, **135** (2020), 533. https://doi.org/10.1140/epjp/s13360-020-00546-x
44. J. Zhang, H. Meng, Z. Zheng, Z. G. Wang, Exact solutions and bifurcation analysis of the time-fractional extended (3+1)-dimensional Kadomtsev-Petviashvili equation with conformable derivative, *Fractals*, **33** (2025), 2550037. https://doi.org/10.1142/s0218348x25500379
45. S. Lynch, *Dynamical systems with applications using Maple*, Boston: Birkhäuser, 2010. https://doi.org/10.1007/978-0-8176-4605-9
46. J. B. Li, H. H. Dai, *On the study of singular nonlinear traveling wave equations: dynamical system approach*, Science Press, 2007.
47. Z. Zheng, H. Meng, J. Zhang, Z. G. Wang, Bifurcations and traveling wave solutions of the space-time fractional coupled Boussinesq equations, *Fractals*, **33** (2025), 25500065. https://doi.org/10.1142/s0218348x25500653
48. M. V. Flamarion, R. J. R. Ribeiro, Solitary waves on flows with an exponentially sheared current and stagnation points, *Q. J. Mech. Appl. Math.*, **76** (2023), 79–91. https://doi.org/10.1093/qjmam/hbac021
49. W. L. Li, X. Liu, Y. H. Lang, Numerical analysis of a nonlinear age-structured HBV model with saturated incidence and spatial diffusion, *Math. Comput. Simul.*, **225** (2024), 250–266. https://doi.org/10.1016/j.matcom.2024.05.022
50. H. L. Xuan, X. L. Cheng, L. L. Yuan, Numerical studies of a class of thermoviscoelastic frictional contact problem described by fractional differential hemivariational inequalities, *J. Sci. Comput.*, **103** (2025), 4. https://doi.org/10.1007/s10915-025-02815-2
51. X. Liu, Z. W. Yang, Numerical analysis of a reaction diffusion susceptible infected susceptible epidemic model, *Comput. Appl. Math.*, **41** (2022), 392. https://doi.org/10.1007/s40314-022-02113-9

AIMS Press